Optical and Quantum Electronics **23** *(1991) 439–459*

Saturable absorption dynamics of DODCI

A. PENZKOFER, W. BÄUMLER
Naturwissenschaftliche Fakultät II-Physik, Universität Regensburg, W-8400 Regensburg, FRG

Received 12 June; revised 16 October; accepted 16 October 1990

The saturable absorption dynamics of DODCI in a femtosecond dye laser is studied theoretically. The N-isomer and P-isomer photoisomerization dynamics is included. The wavelength region between 570 nm and 650 nm is considered where the N-isomer and P-isomer absorption dynamics changes from short-wavelength to long-wavelength S_0–S_1 excitation. The slow saturable absorber DODCI shortens a circulating pulse in a laser oscillator down to femtosecond duration if the gain medium compensates the absorber losses. Fast local relaxation in the S_1-state in the case of short-wavelength excitation and fast level refilling in the S_0^*-state in the case of long-wavelength excitation facilitate the pulse shortening and the background signal suppression.

1. Introduction

The organic dye DODCI (3,3′-diethyloxadicarbocyanine iodide) [1, 2] is widely used as a saturable absorber in passively mode-locked pulsed dye lasers [3, 4] and c.w. dye lasers [5–8]. It is applied in the wavelength region between 574 nm [9] and 645 nm [4]. Especially in a prism balanced colliding-pulse mode-locked rhodamine 6G ring dye laser pulse durations down to 20 fs have been generated around 620 nm using DODCI as the mode-locking dye [10, 11].

Laser excitation of DODCI leads to photoisomerization [2, 6]. The N-isomer mainly present in the ground-state at thermal equilibrium [12] is partially transferred to the P-isomer conformation [13, 14 and references therein]. For DODCI in ethylene glycol the absorption peak of the N-isomer is at 585 nm and that of the P-isomer is at 620 nm [12]. In some papers [3, 11, 15, 16] the bleaching of the ground-state P-isomer absorption is thought to be responsible for the picosecond and femtosecond pulse generation in passively mode-locked rhodamine 6G dye lasers in the wavelength region above 600 nm.

In this paper a detailed numerical analysis of the saturable absorption dynamics of DODCI in the wavelength region between 570 nm and 650 nm is given. The single transit of a pulse through the absorber and the repetitive passage of a pulse circulating in an oscillator are studied. The N-isomer–P-isomer photoisomerization dynamics is included [13, 14]. In the long-wavelength absorption region the bleaching dynamics of the fraction of molecules interacting with the laser light is considered [17, 18]. It is found that the slow saturable absorber is able to shorten nanosecond Gaussian pulses down to femtosecond pulses in multiple passages if the gain medium compensates the absorber losses. The fast relaxation of the excited Franck–Condon level in the S_1-state in the case of short-wavelength excitation, and the fast spectral cross-relaxation in the S_0-ground state in the case of

0306-8919/91 $03.00 + .12

long-wavelength excitation facilitate the pulse shortening and the background light suppression.

2. Theory

The S_0 and S_1 potential energy diagrams of the N- and P-isomer conformations of DODCI have been determined in [12, 13]. The relevant energy level diagrams for the saturable absorption dynamics are displayed in Fig. 1. Depending on the laser wavelength λ_L three different situations occur: Case (a) for $\lambda_L < 598$ nm all N- and P-molecules take part in the absorption process (short-wavelength interaction). The molecules are excited to vibronic Franck–Condon states in the S_1 band. Case (b) for 598 nm $< \lambda_L <$ 631 nm only a fraction of thermally excited N-isomer molecules interacts with the laser light (long-wavelength absorption) while all P-isomer molecules are involved in the absorption process (short-wavelength interaction). Case (c) for $\lambda_L > 631$ nm the long-wavelength absorption situation applies to both the N- and P-isomers.

The rate equations for the three situations are given in the following. The transformations $t' = t - nz/c_0$ and $z' = z$ are used, where t is the time, n the refractive index, z the distance along the propagation direction, and c_0 the vacuum light velocity. The excited state absorption and the absorption anisotropy are neglected (for inclusion see [17]). Excited-state absorption of DODCI has been studied in [19].

For $\lambda_L < 598$ nm (case a) the equations read

$$\frac{\partial N_1}{\partial t'} = -\frac{\sigma_N}{h\nu_L}(N_1 - N_2^*)I_L + k_N(N_2 + N_2^*) + k_{PN}^{10}(N_3 + N_3^*) + k_{PN}^0 N_4 - k_{NP}^0 N_1 \quad (1)$$

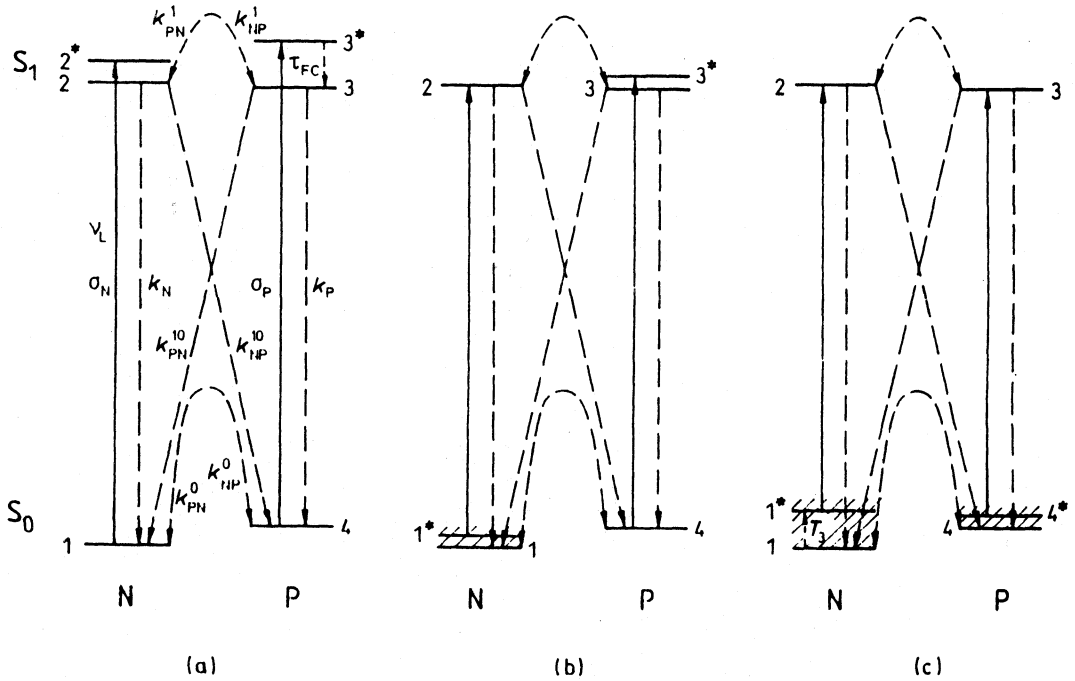

Figure 1 S_0 and S_1 singlet level diagrams of N- and P-isomers of DODCI in ethylene glycol for description of saturable absorption. (a) Short-wavelength S_0–S_1 excitation of N- and P-isomers for $\lambda_L < 598$ nm; (b) Long-wavelength N-isomer excitation and short-wavelength P-isomer excitation for 598 nm $< \lambda <$ 631 nm; (c) Long-wavelength S_0–S_1 excitation of N- and P-isomers for $\lambda_L > 631$ nm.

$$\frac{\partial N_2}{\partial t'} = \frac{N_2^*}{\tau_{FC}} + k_{PN}^1(N_3 + N_3^*)\frac{N_2}{N_2 + N_2^*} - (k_N + k_{NP}^1 + k_{NP}^{10})N_2 \tag{2}$$

$$\frac{\partial N_2^*}{\partial t'} = \frac{\sigma_N}{h\nu_L}(N_1 - N_2^*)I_L - \frac{N_2^*}{\tau_{FC}} + k_{PN}^1(N_3 + N_3^*)\frac{N_2^*}{N_2 + N_2^*} - (k_N + k_{NP}^1 + k_{NP}^{10})N_2^* \tag{3}$$

$$\frac{\partial N_3}{\partial t'} = \frac{N_3^*}{\tau_{FC}} + k_{NP}^1(N_2 + N_2^*)\frac{N_3}{N_3 + N_3^*} - (k_P + k_{PN}^1 + k_{PN}^{10})N_3 \tag{4}$$

$$\frac{\partial N_3^*}{\partial t'} = \frac{\sigma_P}{h\nu_L}(N_4 - N_3^*)I_L - \frac{N_3^*}{\tau_{FC}} + k_{NP}^1(N_2 + N_2^*)\frac{N_3^*}{N_3 + N_3^*} - (k_P + k_{PN}^1 + k_{PN}^{10})N_3^* \tag{5}$$

$$\frac{\partial N_4}{\partial t'} = -\frac{\sigma_P}{h\nu_L}(N_4 - N_3^*)I_L + k_{NP}^{10}(N_2 + N_2^*) + k_P(N_3 + N_3^*) + k_{NP}^0 N_1 - k_{PN}^0 N_4 \tag{6}$$

$$\frac{\partial I_L}{\partial z} = -I_L[\sigma_N(N_1 - N_2^*) + \sigma_P(N_4 - N_3^*)] \tag{7}$$

with the initial conditions $N_1(t' = -\infty, z) = (1 - \rho_{P,th})N$, $N_2(-\infty) = N_2^*(-\infty) = N_3(-\infty) = N_3^*(-\infty) = 0$, $N_4(-\infty, z) = N_{4,th} = \rho_{P,th}N$. N is the total number density of dye molecules. $\rho_{P,th}$ is the thermal population of P-isomers in the S_0-ground state.

For 598 nm $< \lambda_L <$ 631 nm (case b) the equations are

$$\frac{\partial N_1}{\partial t'} = -\frac{\sigma_N}{h\nu_L}(N_1^* - N_2)I_L + k_N N_2 + k_{PN}^{10}(N_3 + N_3^*) + k_{PN}^0 N_4 - k_{NP}^0 N_1 \tag{8}$$

$$\frac{\partial N_1^*}{\partial t'} = -\frac{\sigma_N}{h\nu_L}(N_1^* - N_2)I_L - \frac{N_1^* - \rho_N N_1}{T_3} \tag{9}$$

$$\frac{\partial N_2}{\partial t'} = \frac{\sigma_N}{h\nu_L}(N_1^* - N_2)I_L + k_{PN}^1(N_3 + N_3^*) - (k_N + k_{NP}^1 + k_{NP}^{10})N_2 \tag{10}$$

$$\frac{\partial N_3}{\partial t'} = \frac{N_3^*}{\tau_{FC}} + k_{NP}^1 N_2\frac{N_3}{N_3 + N_3^*} - (k_P + k_{PN}^1 + k_{PN}^{10})N_3 \tag{11}$$

$$\frac{\partial N_3^*}{\partial t'} = \frac{\sigma_P}{h\nu_L}(N_4 - N_3^*)I_L - \frac{N_3^*}{\tau_{FC}} + k_{NP}^1 N_2\frac{N_3^*}{N_3 + N_3^*} - (k_P + k_{PN}^1 + k_{PN}^{10})N_3^* \tag{12}$$

$$\frac{\partial N_4}{\partial t'} = -\frac{\sigma_P}{h\nu_L}(N_4 - N_3^*)I_L + k_{NP}^{10}N_2 + k_P(N_3 + N_3^*) + k_{NP}^0 N_1 - k_{PN}^0 N_4 \tag{13}$$

$$\frac{\partial I_L}{\partial z} = -I_L[\sigma_N(N_1^* - N_2) + \sigma_P(N_4 - N_3^*)] \tag{14}$$

with the initial conditions $N_1(t' = -\infty, z) = (1 - \rho_{P,th})N$, $N_1^*(t' = -\infty, z) = N_1(t' = -\infty, z)\rho_N$, $N_2(-\infty) = N_3(-\infty) = N_3^*(-\infty) = 0$, $N_4(-\infty, z) = N_{4,th}$. ρ_N is

given by

$$\rho_N = \begin{cases} \exp\left[-\dfrac{h(\nu_{12}-\nu_L)}{k_B\vartheta}\right] & \text{for } \nu_{12} > \nu_L \\ 1 & \text{for } \nu_{12} \leqslant \nu_L \end{cases} \tag{15}$$

where ν_{12} is the electronic S_0–S_1 transition frequency of the N-isomers, k_B is the Boltzmann constant, and ϑ is the temperature. The level population N_1 includes N_1^*.

For $\lambda_L > 631$ nm (case c) the equations are

$$\frac{\partial N_1}{\partial t'} = -\frac{\sigma_N}{h\nu_L}(N_1^* - N_2)I_L + k_N N_2 + k_{PN}^{10} N_3 + k_{PN}^{0} N_4 - k_{NP}^{0} N_1 \tag{16}$$

$$\frac{\partial N_1^*}{\partial t'} = -\frac{\sigma_N}{h\nu_L}(N_1^* - N_2)I_L - \frac{(N_1^* - \rho_N N_1)}{T_3} \tag{17}$$

$$\frac{\partial N_2}{\partial t'} = \frac{\sigma_N}{h\nu_L}(N_1^* - N_2)I_L + k_{PN}^{1} N_3 - (k_N + k_{NP}^{1} + k_{NP}^{10})N_2 \tag{18}$$

$$\frac{\partial N_3}{\partial t'} = \frac{\sigma_P}{h\nu_L}(N_4^* - N_3)I_L + k_{NP}^{1} N_2 - (k_P + k_{PN}^{1} + k_{PN}^{10})N_3 \tag{19}$$

$$\frac{\partial N_4}{\partial t'} = -\frac{\sigma_P}{h\nu_L}(N_4^* - N_3)I_L + k_P N_3 + k_{NP}^{10} N_2 + k_{NP}^{0} N_1 - k_{PN}^{0} N_4 \tag{20}$$

$$\frac{\partial N_4^*}{\partial t'} = -\frac{\sigma_P}{h\nu_L}(N_4^* - N_3)I_L - \frac{(N_4^* - \rho_P N_4)}{T_3} \tag{21}$$

$$\frac{\partial I_L}{\partial z'} = -I_L[\sigma_N(N_1^* - N_2) + \sigma_P(N_4^* - N_3)] \tag{22}$$

with the initial conditions $N_1(t' = -\infty, z) = (1 - \rho_{P,th})N$, $N_1^*(t' = -\infty, z) = \rho_N N_1(t' = -\infty, z)$, $N_2(-\infty) = N_3(-\infty) = 0$, $N_4(t' = -\infty, z) = N_{4,th}$, $N_4^*(t' = -\infty, z) = \rho_P N_4(t' = -\infty, z)$. The level populations N_1 include N_1^* and N_4 include N_4^*. ρ_P is given by

$$\rho_P = \begin{cases} \exp\left[-\dfrac{h(\nu_{43}-\nu_L)}{k_B\vartheta}\right] & \text{for } \nu_{43} > \nu_L \\ 1 & \text{for } \nu_{43} \leqslant \nu_L \end{cases} \tag{23}$$

where ν_{43} is the electronic S_0–S_1 transition frequency of the P-isomers.

σ_N and σ_P are the ground-state absorption cross-sections of the interacting N- and P-isomers, respectively. τ_{FC} is the relaxation time of the excited Franck–Condon states in the S_1-band. T_3 is the spectral cross-relaxation time (thermal redistribution) in the S_0-band. $k_N = \tau_N^{-1}$ and $k_P = \tau_P^{-1}$ are the inverse fluorescence lifetimes of the N- and P-isomers, respectively. The N- to P- (P- to N-) transfer rate in the ground-state is k_{NP}^0 (k_{PN}^0). The transfer rates from N to P and P to N in the S_1-state are k_{NP}^1 and k_{PN}^1, respectively. The S_1 to S_0 inter-isomer relaxation rates are k_{NP}^{10}(N → P) and k_{PN}^{10}(P → N).

The initial small signal transmission through a sample of length l is given by

$$T_{0,i} = \exp(-\sigma_i N l) \tag{24}$$

with

$$\sigma_i = (1 - \rho_{P,th})\rho_N\sigma_N + \rho_{P,th}\rho_P\sigma_P \tag{25}$$

The absorption bleaching may be characterized by saturation intensities. One has to distinguish between the saturation intensity $I_{S,f}$ of fast saturable absorbers (absorption recovery time $\tau <$ pulse duration Δt_L) and the saturation intensity $I_{S,s}$ of slow saturable absorbers ($\tau > \Delta t_L$). For three-level absorbers with fast intermediate excited level the fast saturation intensity is [20] $I_{S,f} = h\nu_L/\sigma\tau$, where σ is the absorption cross-section. In analogy the slow saturation intensity is $I_{S,s} = h\nu_L/\sigma\Delta t_L$. For the bleaching of the N-isomers and P-isomers of DODCI the fast and slow saturation intensities are defined by

$$I_{S,f} = \frac{h\nu_L}{\rho_N(1 - \rho_{P,th}) + \rho_{P,th}\rho_P}\left[\frac{\rho_N(1 - \rho_{P,th})}{\sigma_N\tau_N} + \frac{\rho_{P,th}\rho_P}{\sigma_P\tau_P}\right] \tag{26}$$

and

$$I_{S,s} = \frac{h\nu_L}{\Delta t_L[\rho_N(1 - \rho_{P,th}) + \rho_{P,th}\rho_P]}\left[\frac{\rho_N(1 - \rho_{P,th})}{\sigma_N} + \frac{\rho_{P,th}\rho_P}{\sigma_P}\right] \tag{27}$$

In the build-up process of femtosecond pulses in a passively mode-locked dye laser oscillator the absorption dynamics of DODCI changes from fast saturable absorption of nanosecond and subnanosecond pulses in an early stage of pulse development to slow saturable absorption of picosecond and femtosecond pulses in a final stage of pulse development.

3. Dye parameters

Most parameters entering Equations 1 to 27 have been determined previously. The parameters independent of the laser wavelength are listed in Table 1. The absorption cross-sections of the molecules interacting with the laser light are depicted in Fig. 2a [13]. It should be noted that in the long-wavelength absorption region the absorption cross-sections are equal to the stimulated emission cross-sections [17, 18].

The dye number density needed for a fixed small-signal initial transmission is

$$N = \frac{-\ln(T_{0,i})}{\sigma_i l} \tag{28}$$

TABLE 1 Parameters of DODCI in ethylene glycol at room temperature ($\vartheta \approx 295$ K).

Parameter	Value	Ref.
$k_N(s^{-1})$	7.75×10^8	[13]
$k_P(s^{-1})$	7×10^8	[13]
$\tau_{FC}(s)$	9.5×10^{-13}	[21]
$\rho_{P,th}$	0.029	[12]
$\tilde{\nu}_{12}(cm^{-1})$	16710	[13]
$\tilde{\nu}_{43}(cm^{-1})$	15840	[13]
$k^0_{NP}(s^{-1})$	15	[13, 22, 23]
$k^0_{PN}(s^{-1})$	465	[14]

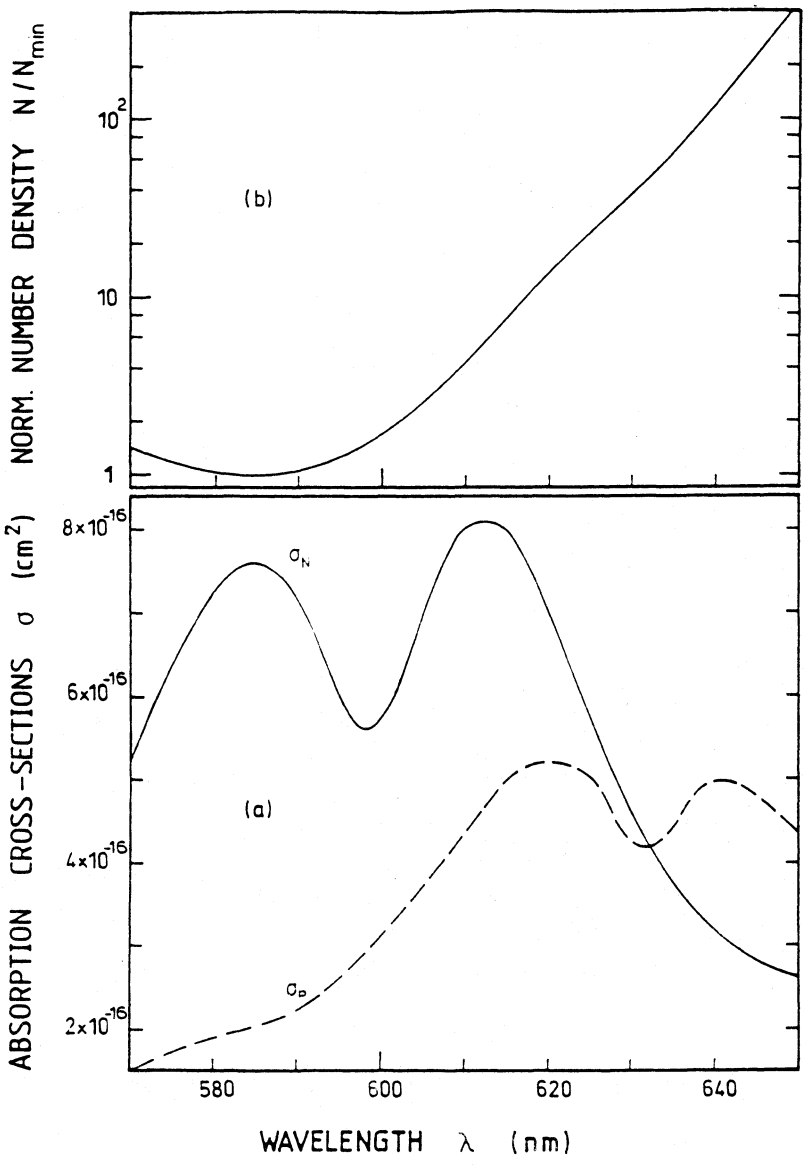

Figure 2 (a) Absorption cross-sections σ_N and σ_P of the N- and P-isomers interacting with laser light (from [13, 14]). (b) Normalized number density of dye molecules needed for constant transmission versus wavelength $N(\lambda)/N_{min} = \sigma_{i,max}/\sigma_i(\lambda)$, see Equations 25 and 28.

(see Equations 24 and 25). The total number density N is wavelength dependent. The ratio $N/N_{min} = \sigma_{i,max}/\sigma_i$ versus wavelength is plotted in Fig. 2b. N_{min} occurs at $\lambda = 585$ nm were the effective initial absorption cross-section σ_i is maximal. For $\lambda \gtrsim 600$ nm. N rises strongly because only molecules excited thermally contribute to the absorption.

Concerning the photoisomerization rates, only $k_{NP}^{tr} = k_{NP}^{1} + k_{NP}^{10}$ and $k_{PN}^{tr} = k_{PN}^{1} + k_{PN}^{10}$ are known [14] and depicted in Fig. 3 as a function of wavelength. The influence of the isomerization path (S_1-state N-P intraband isomerization or S_1-state to S_0-state N-P interband isomerization) on the absorption dynamics is analysed below in Section 4.1.3. The spectral cross-relaxation time T_3 in the S_0-band is unknown. T_3 is expected to be in the

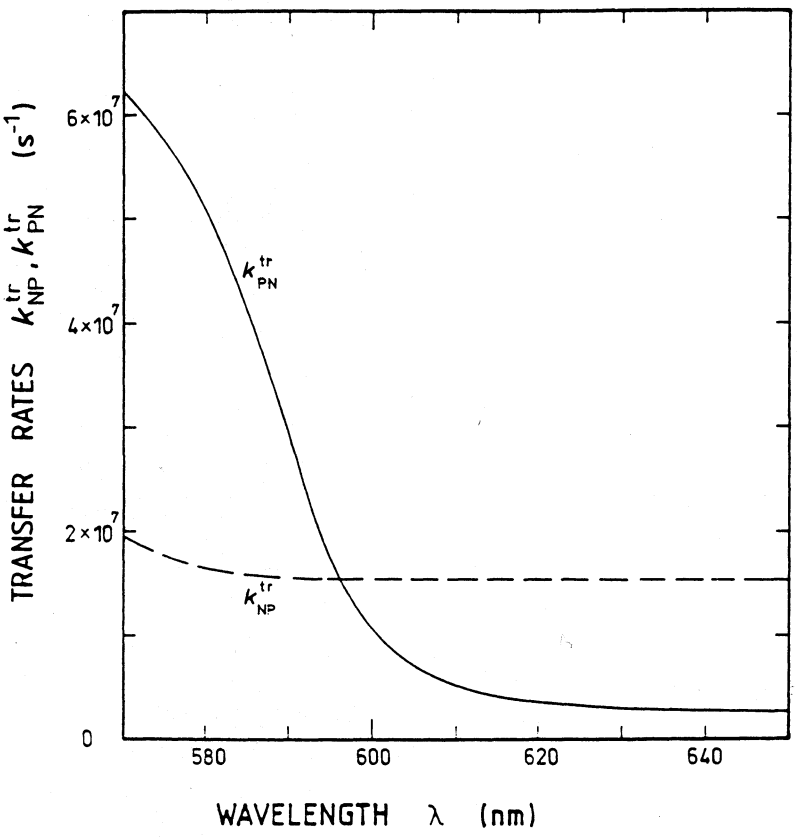

Figure 3 Photoisomerization transfer rates k^{tr}_{NP} for transition from S_1-state N-isomer to P-isomer, and k^{tr}_{PN} for transition from S_1-state P-isomer to N-isomer (from [14]).

picosecond region [24]. The dependence of the absorption dynamics on T_3 is studied below in Section 4.1.1.

4. Simulations

For picosecond and femtosecond pulse generation DODCI in ethylene glycol is a slow saturable absorber because the absorption recovery times of the N-isomer, $\tau_N = k_N^{-1} \approx 1.3$ ns, and the P-isomer, $\tau_P = k_P^{-1} \approx 1.4$ ns, are long compared to the laser pulse durations.

For a single passage through the absorber the influences of the spectral cross-relaxation time T_3, of the Franck–Condon relaxation time τ_{FC}, and of the photoisomerization path are analysed. Additionally the difference in pulse shortening of nanosecond pulses (fast saturable absorption) and picosecond pulses (slow saturable absorption) is studied. The wavelength region between 570 nm and 650 nm is considered. In this region the N-isomer and P-isomer absorption dynamics changes from short-wavelength absorption to long-wavelength absorption (Fig. 1).

The pulse shortening action of the slow saturable absorber in many roundtrips is studied where the amplifying medium only recovers the absorbed energy without any pulse shaping action. The importance of a fast Franck–Condon relaxation time τ_{FC} in the S_1-state and of a fast spectral cross-relaxation time T_3 in the ground-state on pulse shortening and background signal suppression is analysed.

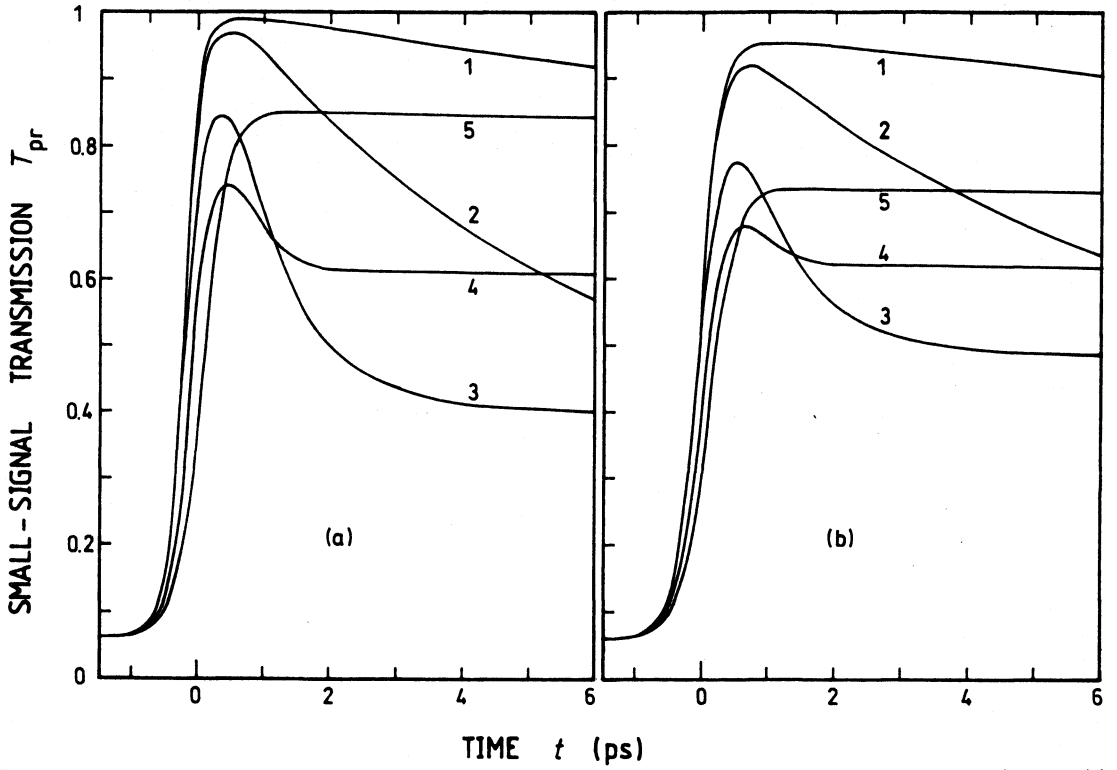

Figure 4 Small-signal probe pulse transmission at pump laser frequency for single passage through saturable absorber. Pump pulse parameters are duration Δt_L = 1 ps, Gaussian shape, peak intensity $I_{0L} = 2 \times 10^9 \text{W cm}^{-2}$ and wavelength λ_L = (a) 590 nm and (b) 640 nm. Dye parameters are taken from Figs 2 and 3 and Table 1 except T_3 and τ_{FC}. The initial small-signal transmission is $T_0 = 0.063$. (a) Variation of τ_{FC} (level scheme of Fig. 1a). The curves belong to τ_{FC} = (1) 100 ps, (2) 10 ps, (3) 1 ps, (4) 0.3 ps and (5) <0.1 ps. (b) Variation of T_3 (level scheme of Fig. 1c). The curves belong to T_3 = (1) 100 ps, (2) 10 ps, (3) 1 ps, (4) 0.3 ps and (5) <0.1 ps.

4.1. Single passage through absorber

4.1.1. Dependence on spectral cross-relaxation time

The influence of the spectral cross-relaxation time T_3 is studied for the experimental situation of laser wavelength λ_L = 640 nm, pulse duration Δt_L = 1 ps and S_1-state intraband photoisomerization where $k^{tr}_{NP} = k^{I}_{NP}$ and $k^{tr}_{PN} = k^{I}_{PN}$ (level diagram of Fig. 1c). The single-pass small-signal transmission is set to $T_0 = 0.063$. The input pulse shape is assumed to be Gaussian, i.e. $I_L(t') = I_{0L} \exp[-(t'/t_0)^2]$ with $t_0 = \Delta t_L/[2(\ln 2)^{1/2}]$. T_3 is varied.

The small-signal transmission versus time is displayed in Fig. 4b for an input peak pulse intensity of $I_{0L} = 2 \times 10^9 \text{W cm}^{-2}$. The spectral cross-relaxation time T_3 is varied. For $T_3 < \tau$ the absorption recovery is enhanced by the finite spectral cross-relaxation time and the background suppression is enforced (see below). In the case of $T_3 \leqslant 0.1\Delta t_L$ the absorber behaves like a three-level system with fast intermediate state and the background suppression action of T_3 is lost.

The time integrated transmission curves, $T_{TI} = \int_{-\infty}^{\infty} I_L(t', l)\mathrm{d}t' / \int_{-\infty}^{\infty} I_L(t', 0)\mathrm{d}t'$, versus input peak intensity I_{0L} are shown in Fig. 5b. Curve 1 applies to $T_3/\Delta t_L \geqslant 10$, curve 2 belongs to $T_3/\Delta t_L = 1$, and curve 3 is obtained for $T_3/\Delta t_L \leqslant 0.1$. For short spectral cross-relaxation times the bleaching is reduced because of refilling the S_0-state levels 1* and 4* within the laser pulse duration.

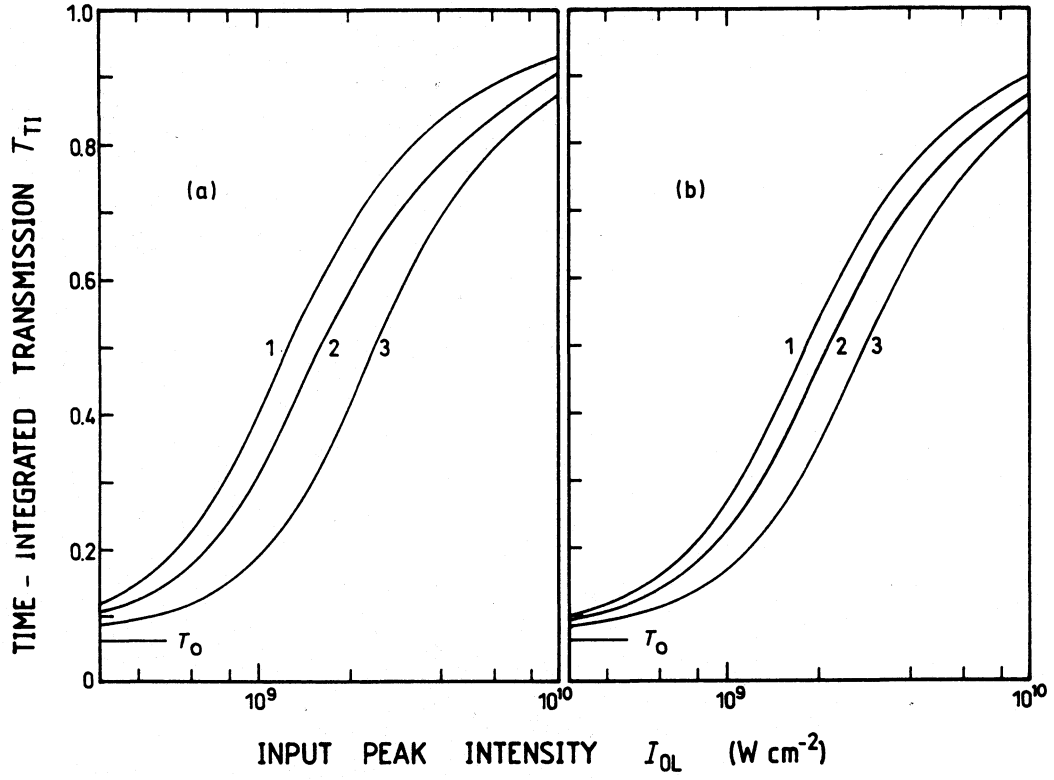

Figure 5 Time-integrated transmission versus input peak intensity for single passage through saturable absorber. Gaussian input pulse of 1 ps duration. Small signal-transmission $T_0 = 0.063$. (a) Dye parameters belong to $\lambda_L = 590$ nm except τ_{FC} (1) $\geqslant 10$ ps, (2) $= 1$ ps and (3) $\leqslant 0.1$ ps. (b) Dye parameters belong to $\lambda_L = 640$ nm except T_3 (1) $\geqslant 10$ ps, (2) $= 1$ ps and (3) $\leqslant 0.1$ ps.

The pulse shortening ratio $\Delta t_{L,out}/\Delta t_L$ versus input peak intensity is depicted in Fig. 6b. The optimum pulse shortening intensity increases slightly for shorter spectral cross-relaxation time values. The optimum shortening ratio is nearly independent of T_3.

The pulse shape asymmetry $\Delta t_+/\Delta t_-$ of the transmitted pulses versus pump pulse peak intensity is plotted in Fig. 7b. Δt_+ is the half-width at half maximum HWHM of the trailing part of the pulse, and Δt_- is the HWHM of the leading part of the pulse ($\Delta t_{L,out} = \Delta t_+ + \Delta t_-$). For input peak intensities $I_{0L} \lesssim 3I_{S,s}$ ($I_{S,s} \approx 4.3 \times 10^8$ W cm^{-2}) the trailing halfwidth is shorter than the rising half-width, for $I_{0L} \gtrsim 3I_{S,s}$ the trailing part is broadened compared to the leading part, and at high intensities $I_{0L} \gg I_{S,s}$ the trailing and rising halfwidths become equal ($\Delta t_+/\Delta t_- \approx 1$). The asymmetry behaviour depends slightly on $T_3/\Delta t_L$.

The shift of the peak position t_P of the transmitted pulse versus input peak intensity is shown in Fig. 8b. The shift is maximal around $I_{0L} \approx 3I_{S,s}$. The behaviour is similar for the different T_3 values.

4.1.2. Dependence on Franck–Condon relaxation time

The Franck–Condon relaxation τ_{FC} in the S_1-state of DODCI in ethylene glycol is known experimentally ($\tau_{FC} = 0.95$ ps [21], see Table 1). In order to study the influence of τ_{FC} on the slow saturable absorption dynamics of DODCI, τ_{FC} is varied and influences on the small-signal transmission T_{pr} (Fig. 4a) the time-integrated pump pulse transmission T_{TI}

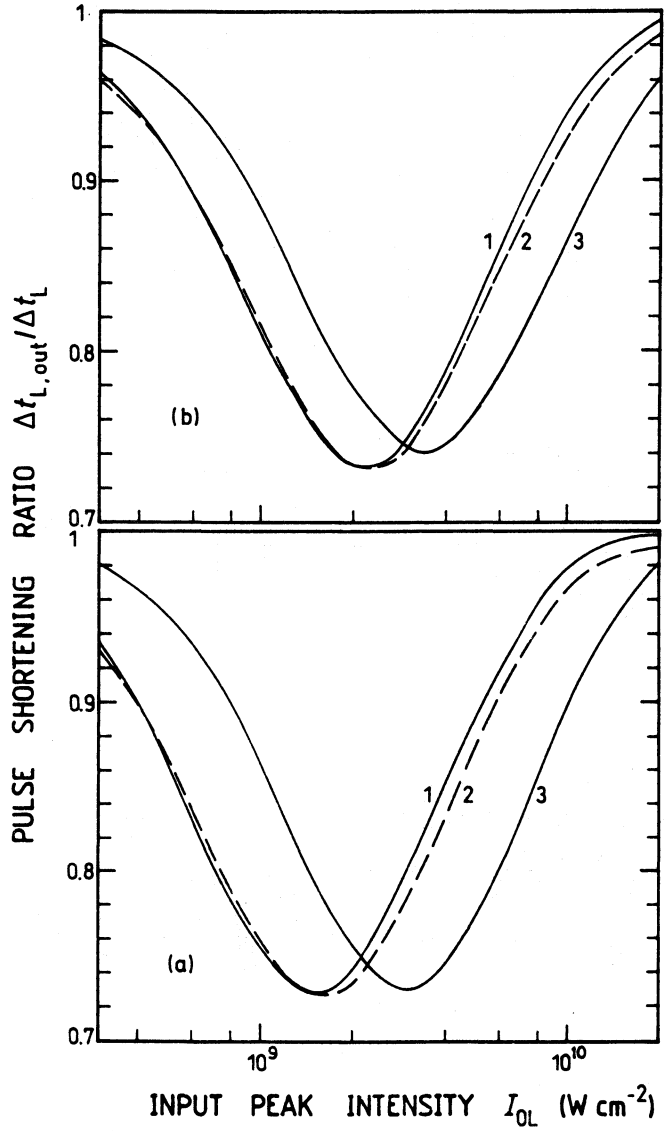

Figure 6 Pulse shortening ratio versus input peak intensity for single passage through saturable absorber. Same pulse and dye parameters as in Fig. 5.

(Fig. 5a), the pulse-shortening ratio $\Delta t_{L,out}/\Delta t_L$ (Fig. 6a), the pulse asymmetry ratio $\Delta t_+/\Delta t_-$ (Fig. 7a), and the temporal intensity peak position t_P/t_0 (Fig. 8a) are illustrated. The influence of τ_{FC} is similar to the influence of T_3.

4.1.3. Dependence on photoisomerization path

The curves in the Figs 4 to 8 have been calculated for the S_1-band intra-isomerization path $k^{tr}_{NP} = k^{1}_{NP}$ and $k^{tr}_{PN} = k^{1}_{PN}$. Practically the same curves are obtained for the S_1–S_0 inter-isomerization path $k^{tr}_{NP} = k^{10}_{NP}$ and $k^{tr}_{PN} = k^{10}_{PN}$ (curves coincide within linewidth).

4.1.4. Dependence on laser wavelength

Across the wavelength region from 570 to 650 nm the absorption dynamics changes from short-wavelength absorption of N- and P-isomers (Fig. 1a) via long-wavelength N-isomer and short-wavelength P-isomer absorption (intermediate region, Fig. 1b) to long-wavelength

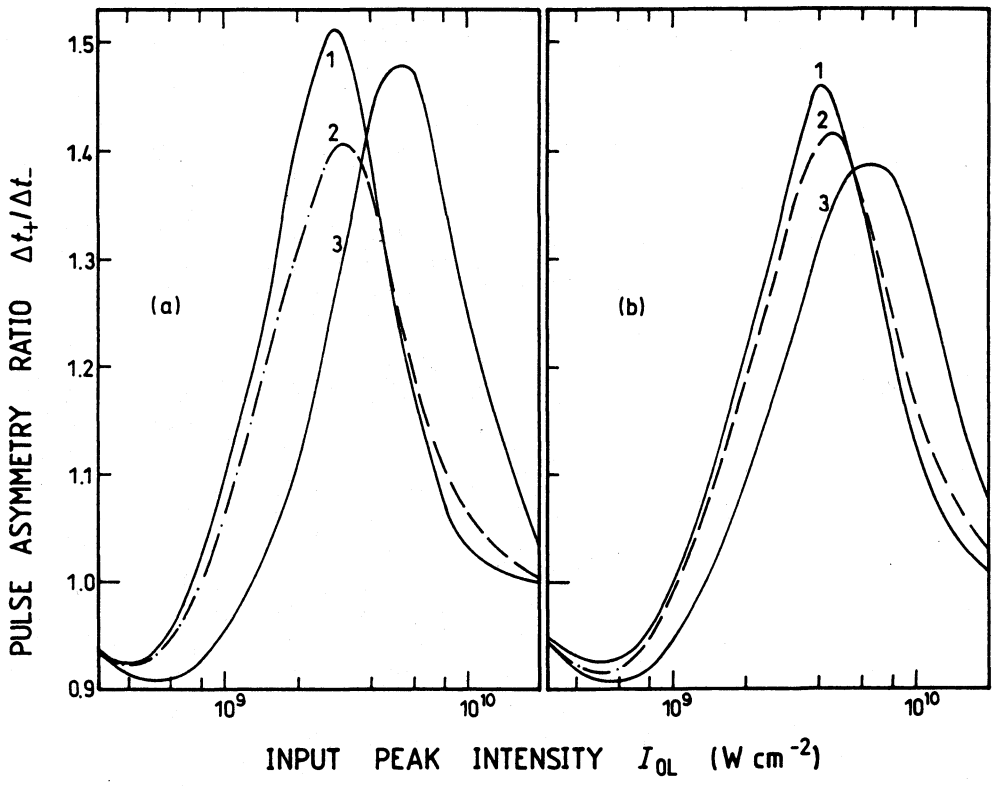

Figure 7 Pulse asymmetry ratio $\Delta t_+/\Delta t_-$ versus input peak intensity for single passage through saturable absorber. Same pulse and dye parameters as in Fig. 5.

N- and P-isomer absorption (Fig. 1c). Additionally the absorption cross-sections σ_P and σ_N (Fig. 2) and the photoisomerization rates k_{NP}^{tr} and k_{PN}^{tr} (Fig. 3) vary with wavelength.

The wavelength dependence of the slow saturable absorption of DODCI is shown in Fig. 9 by the solid curves. The single passage of a Gaussian input pulse is considered. The small-signal transmission is kept constant at $T_0 = 0.063$, the input pulse duration is set to $\Delta t_L = 1$ ps, and the spectral cross-relaxation time is set to $T_3 = 1$ ps. The other parameters are listed in Table 1. Part 9a displays the optimum pulse shortening ratio $\Delta t_{L,out}^{opt}/\Delta t_L$. The temporal peak position t_P^{opt} of the transmitted pulse in the case of optimum pulse shortening is shown in Fig. 9b, and the input peak intensity I_{0L}^{opt} for optimum pulse shortening is shown in Fig. 9c.

The dash–dotted curve of Fig. 9a presents the optimum pulse shortening ratio in the case of fast saturable absorption of DODCI. The input pulse duration is increased to $\Delta t_L = 10$ ns while the other parameters are kept unchanged. For this example the single-pass pulse shortening action in the fast saturable absorption regime is approximately a factor of 1.03 more effective than in the slow absorption regime. The optimum input laser intensity is lowered a factor of 1000 which is approximately the ratio of the saturation intensities $I_{S,f}/I_{S,s}(\Delta t_L = 1$ ps). (Note that $I_{S,f}$ depends on the absorption recovery time and $I_{S,s}$ on the pulse duration).

4.2. Repetitive transits through absorber

The pulse development in repetitive transits through DODCI in a laser oscillator is studied. The initial pulse is assumed to have a Gaussian temporal profile. The influence of a constant

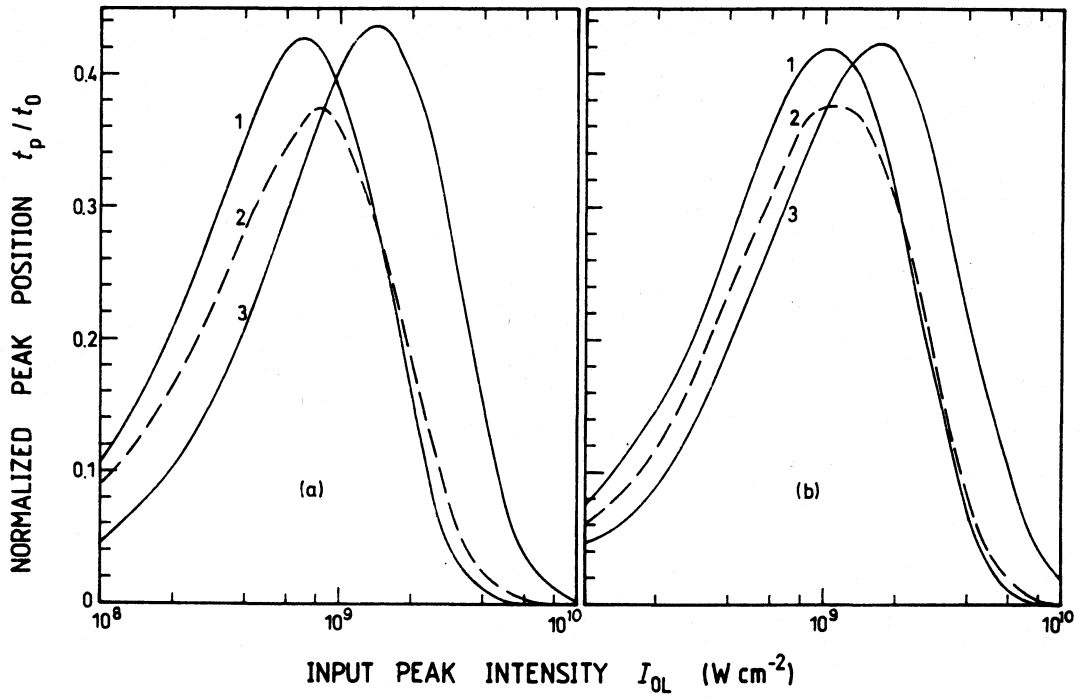

Figure 8 Normalized temporal position of intensity peak of transmitted pulse, t_p/t_0, versus input peak intensity for single passage through saturable absorber. Same pulse and dye parameters as in Fig. 5.

background level is tested. The resonator round-trip time is set to $t_R = 10\,\text{ns}$. The gain medium retains the pulse energy constant, i.e. $I_{0L,j}\Delta t_{L,j} = \text{const}$, where $I_{0L,j}$ is the input peak intensity and $\Delta t_{L,j}$ is the input pulse duration at the j-th transit through the absorber. The pulse shaping action of the amplifying medium by the gain saturation [25–30] is not included.

First the steady-state consequences of the photoisomerization dynamics are discussed, then the continuing pulse shortening action of the slow saturable absorber in succeeding transits is analysed and finally examples of the pulse development as a function of the number of transits are given.

4.2.1. *Influence of photoisomerization dynamics*

The laser pulses passing through DODCI lead to an accumulation of P-isomers due to photoisomerization [14]. The wavelength dependent maximum P-isomer mole fraction, $x^0_{P,max} = N_{4,max}/N$, approached in repetitive excitation with intense light pulses is shown by the dashed curve in Fig. 10a (redrawn from [14]). The P-isomer accumulation changes the absorption coefficient from $\alpha_i = (1 - \rho_{P,th})\rho_N\sigma_N + \rho_{P,th}\rho_P\sigma_P$ (Equation 25) to $\alpha_f = (1 - x^0_{P,max})\rho_N\sigma_N + x^0_{P,max}\rho_P\sigma_P$. The ratio α_f/α_i versus wavelength λ is shown by the solid curve in Fig. 10a. For $\lambda < 603.5\,\text{nm}$ $\rho_N\sigma_N$ is larger than $\rho_P\sigma_P$ (see Fig. 6a of [14]) and therefore the P-isomer accumulation reduces the absorption ratio α_f/α_i and the optimum pulse shortening effect is lowered (see below and Fig. 9a). Above $\lambda = 603.5\,\text{nm}$ $\rho_N\sigma_N$ is lower than $\rho_P\sigma_P$ and the absorption ratio α_f/α_i and the optimum pulse shortening effect (Fig. 9a) are increased. The absorption ratio α_f/α_i is highest at 620 nm. Above 640 nm α_f/α_i becomes equal to 1 because $x^0_{P,max}$ becomes equal to $\rho_{P,th}$.

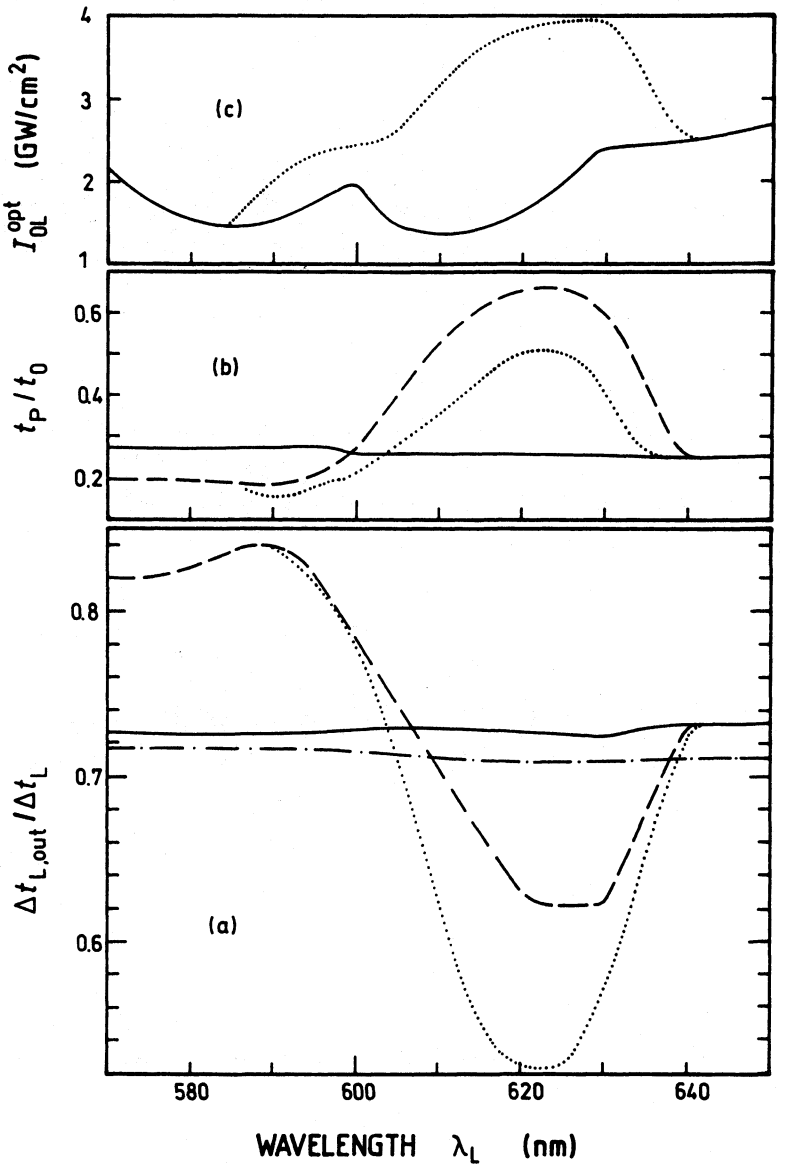

Figure 9 Wavelength dependent pulse shortening. Gaussian input pulses of 1 ps duration. Initial small-signal transmission $T_{0,i}$ = 0.063. Spectral cross-relaxation time T_3 = 1 ps. Franck–Condon relaxation time τ_{FC} = 0.95 ps. (a) Single-pass pulse shortening ratio $\Delta t_{L,out}/\Delta t_L$. (b) Temporal position of intensity peak of transmitted pulse. (c) Peak intensities for optimum pulse shortening. (——) optimum initial pulse shortening; (– – –) pulse shortening after maximum P-isomer accumulation for optimum initial intensity values. (· · · ·) optimum final pulse shortening. The (—·—) curve in (a) illustrates the optimum initial pulse shortening for Δt_L = 10 ns (fast saturable absorption). In this case $t_P/t_0 \approx 0.05$ and $I_{0L}^{opt} \approx 10^6$ W cm^{-2}.

The characteristic isomerization time τ_{iso} needed for effective accumulation of P-isomers at the laser intensity $I_{0L,i}^{opt}$ of initial optimum pulse shortening (solid curve in Fig. 9c) is shown in Fig. 10b. τ_{iso} is given by

$$\tau_{iso} = \frac{N_{4,max} - N_{4,th}}{N_4(t_R) - N_{4,th}} t_R = \frac{N(x_{P,max}^0 - \rho_{P,th})}{N_4(t_R) - \rho_{P,th} N} t_R \qquad (29)$$

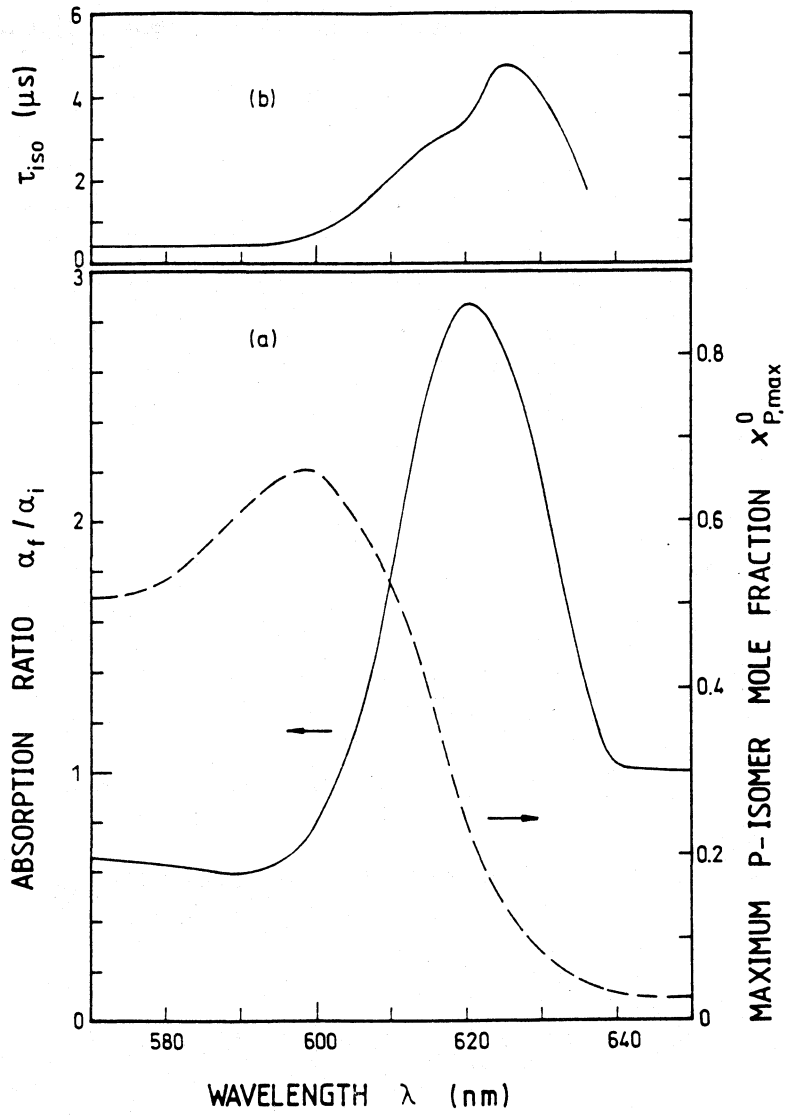

Figure 10 Absorption change due to photoisomerization. (a) (——) curve represents ratio of absorption coefficients. α_f is steady state absorption coefficient due to maximum P-isomer accumulation. α_i is absorption coefficient of dye before laser excitation. (– – –) maximum possible P-isomer mole fraction, $x^0_{P,max}$, due to photoisomerization (from [14]). (b) Characteristic build-up time, τ_{iso}, of P-isomer accumulation for repetitive bleaching of saturable dye. Initial small-signal transmission $T_{0,i}$ = 0.063. Initial input pulse duration is Δt_L = 1 ps. Peak pulse intensity is given by (——) curve in Fig. 9c.

where $N_4(t_R)$ is the population of the S_0–P-isomer level after one round-trip. Equation 29 is obtained by calculating the first derivative of $N_4(t = jt_R) = \{\rho_{P,th} + (x^0_{P,max} - \rho_{P,th})[1 - \exp(jt_R/\tau_{iso})]\}N$. For $\lambda \lesssim 600$ nm the N-isomer absorption dominates and causes the fast P-isomer accumulation. Above 640 nm no P-isomer accumulation occurs ($x^0_{P,max} \approx \rho_{P,th}$). Around 625 nm the time τ_{iso} needed for approaching the saturation P-isomer accumulation is longest.

The change of the pulse shortening behaviour due to P-isomer accumulation is illustrated in Fig. 9. The dashed curve of Fig. 9a belongs to the final situation of $x^0_P = x^0_{P,max}$ and d

$I_{0L} = I_{0L,i}^{opt}$. Below 607 nm the pulse shortening is less efficient because of reduced absorption (Fig. 10a). Between 607 nm and 640 nm the pulse shortening is more efficient because of increased absorption. The temporal peak position t_P of the transmitted pulse is shown by the dashed curve in Fig. 9b.

The P-isomer accumulation shifts the optimum input pulse intensity to $I_{0L,f}^{opt}$ which is shown by the dotted curve in Fig. 9c. The obtained pulse shortening at $I_{0L,f}^{opt}$ is displayed by the dotted curve in Fig. 9a, and the temporal peak position of the transmitted pulse is shown by the dotted curve in Fig. 9b.

The curves in Fig. 9a indicate that the pulse shortening action of DODCI in a c.w. mode-locked dye laser is highest in the wavelength region between 605 and 640 nm. It should be noted that the shortest pulses of 20 fs were generated around 620 nm in a prism balanced colliding pulse mode-locked CPM rhodamine 6G dye laser with DODCI/ethylene glycol as saturable absorber [10, 11].

4.2.2. Continuous pulse shortening in repetitive transits

Three examples of the pulse development versus the number of transits are displayed in Fig. 11. The initial pulses are assumed to be Gaussian of 1 ps duration. The solid curves belong to an initial dye transmission $T_{0,i} = 0.9$ and the dashed and the dash–dotted curves are calculated for $T_{0,i} = 0.063$. The dye parameters at $\lambda_L = 620$ nm are applied. $T_3 = 1$ ps and $\tau_{FC} = 0.95$ ps are used for the solid and dashed curves. The dash–dotted curves are calculated for $T_3 = \tau_{FC} = 1$ ns. The pulses are reamplified after each absorber passage to peak intensities of $I_{0L,j} = 6 \times I_{S,s}$ in the case of $T_{0,i} = 0.9$ and to $I_{0L,j} = 8 \times I_{S,s}$ in the case of $T_{0,i} = 0.063$ ($I_{S,s}$ is inversely proportional to pulse duration, see Equation 26). The effect of dye replacement in the absorber jet is taken into consideration by setting the N- and P-isomer number densities after each round-trip to

$$N_1[(j+1)t_R] = N_1(jt_R)\frac{d - vt_R}{d} + N(1 - \rho_{P,th})\frac{vt_R}{d} \tag{30}$$

and

$$N_4[(j+1)t_R] = N_4(jt_R)\frac{d - vt_R}{d} + N\rho_{P,th}\frac{vt_R}{d} \tag{31}$$

where d is the laser beam diameter and v is the flowing speed of the absorber ($d = 7\,\mu$m and $v = 7\,\text{ms}^{-1}$ are used in calculations).

Figure 11a shows the mole fraction of P-isomers $x_{P,j}^0$. The limiting value $x_{P,max}^0$ is not reached because of the absorber replacement in the fast flowing jet. The pulse durations are displayed in Fig. 11b. For the first few round-trips the pulse shortening is strongest. The pulse shortening ratio $\Delta t_{L,j+1}/\Delta t_{L,j} = \Delta t_{L,j,out}/\Delta t_{L,j}$ reduces with the number of transits but it does not come to an end. (In real passively mode-locked c.w. dye lasers, the pulse shortening is limited by the group velocity dispersion in the absorber and gain jet [7] and the finite gain width of the active medium.)

Comparison of the dashed curve ($T_3 = 1$ ps and $\tau_{FC} = 0.95$ ps) and the dash–dotted curve ($T_3 = \tau_{FC} = 1$ ns) of Fig. 11b indicates that the fast Franck–Condon relaxation τ_{FC} in the S_1-state and the fast spectral-cross-relaxation T_3 in the S_0-ground-state facilitate the pulse-shortening (partial fast absorption recovery).

The time position of the peak intensity of the circulating pulse $t_{P,j}$ is displayed in Fig. 11c. It shifts continuously to the trailing part with the number of transits. The pulse asymmetry ratio $(\Delta t_+/\Delta t_-)_j$ increases with the number of round-trips as is shown in Fig. 11d.

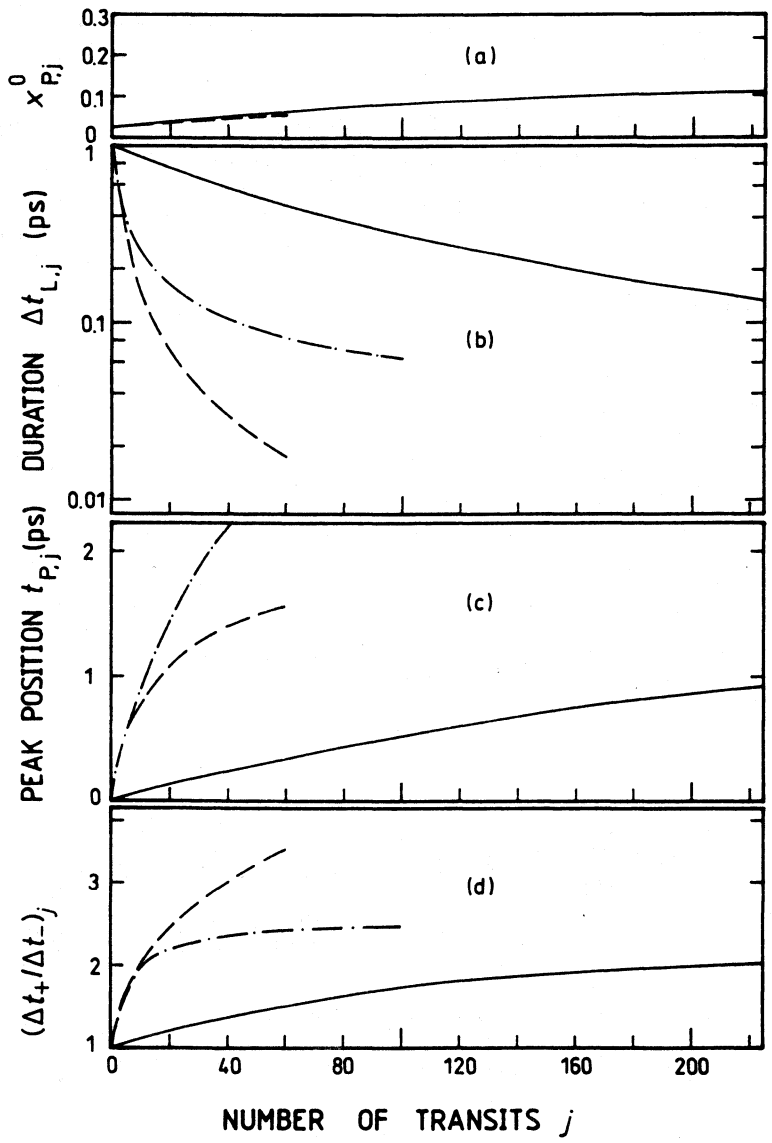

Figure 11 Pulse development in multiple transits through saturable absorber. Initial pulse has Gaussian shape and 1 ps duration. Dye parameters belong to λ_L = 620 nm with T_3 = 1 ps (τ_{FC} = 0.95 ps). (——) curves are calculated for $T_{0,i}$ = 0.9 and $I_{0L,j} = 6I_{S,s}(\Delta t_{L,j})$. (– – –) are calculated for $T_{0,i}$ = 0.063 and $I_{0L,j} = 8I_{S,s}(\Delta t_{L,j})$. The absorber jet parameters are flowing speed v = 7 m s^{-1} and laser spot size d = 7 μm. The (—·—) curves are calculated for the same parameters as the (– – –) curves except $T_3 = \tau_{FC}$ = 1 ns. (a) Mole fraction of P-isomers $x^0_{P,j}$. (b) Pulse duration $\Delta t_{L,j}$. (c) Temporal position of intensity maximum $t_{P,j}$. (d) Pulse asymmetry $(\Delta t_+/\Delta t_-)_j$.

The continuing pulse shortening of a Gaussian pulse by repetitive passage through a slow saturable absorber has its origin in the absorption of the leading part shifting the pulse peak position more and more to the trailing edge where the wings become steeper and steeper. The situation is illustrated by the solid curves in Fig. 12a where a Gaussian pulse $I(t) = I_{0L} \exp(-t^2/t_0^2)$ is displayed out to t/t_0 = 5.5. The time increments $\delta t_{1/2}(t)$ needed to reduce the intensity to half its value at position t normalized to the time increment $\delta t_{1/2}(0)$ are shown by the dashed curve. The curve is determined by the relation

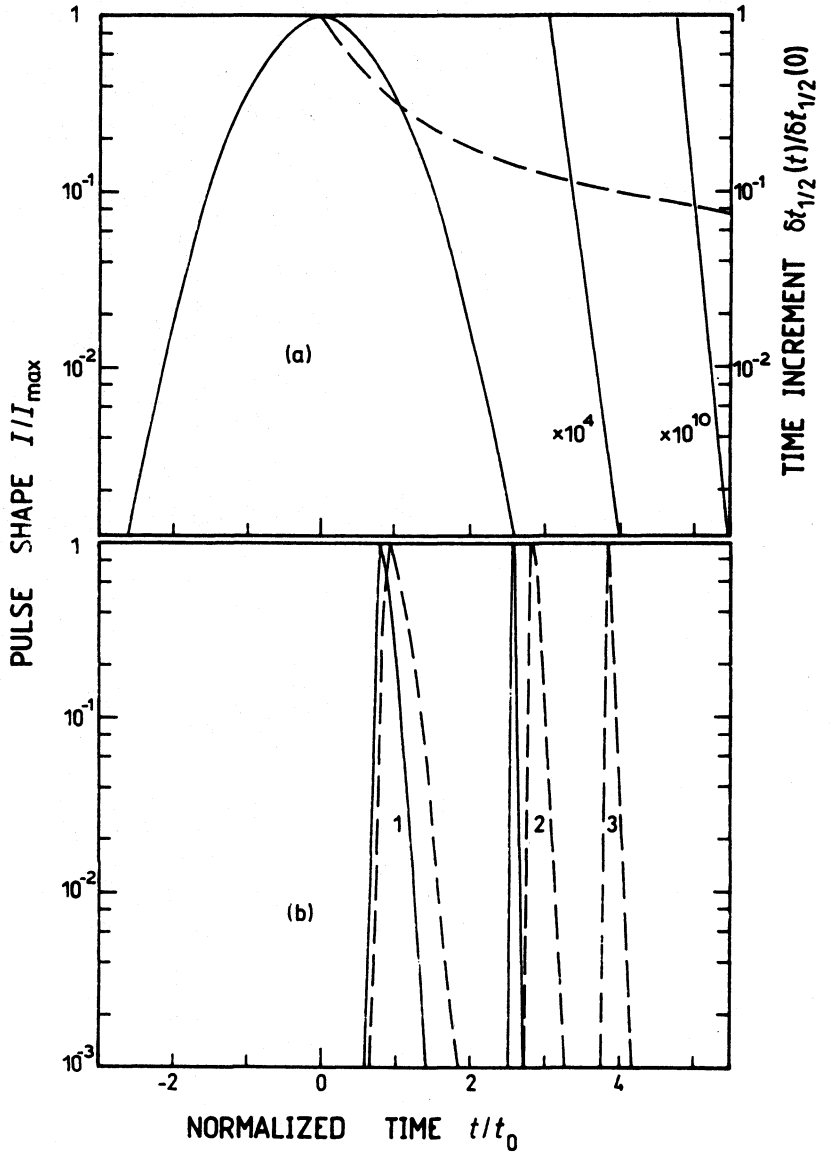

Figure 12 Illustration of repetitive pulse shortening action of slow saturable absorber. (a) (——) shows input Gaussian pulse shape; (– – –) normalized time increment $\delta t_{1/2}(t)/\delta t_{1/2}(0)$ where $\delta t_{1/2}(t)$ is time increment at t needed to reduce envelope value of Gaussian pulse by a factor of two; (b) (——) curves show shapes of pulses belonging to (– – –) curves of Fig. 11 after (1) 10 transits and (2) 60 transits. (– – –) show shapes of pulses belonging to (—·—) curves of Fig. 11 after (1) 10 transits, (2) 60 transits and (3) 100 transits.

$\exp[-(t + \delta t_{1/2})^2/t_0^2] = 0.5 \exp(-t^2/t_0^2)$ leading to $\delta t_{1/2}(0) = [-\ln(0.5)]^{1/2} t_0$ and $\delta t_{1/2}(t) = [t^2 - \ln(0.5)t_0^2]^{1/2} - t$. For $t/t_0 \gtrsim 10$ the time increment is given approximately by $\delta t_{1/2}(t) \approx -\ln(0.5)t_0^2/2t$ and the ratio becomes

$$\delta t_{1/2}(t)/\delta t_{1/2}(0) \approx [-\ln(0.5)]^{1/2} t_0/2t \tag{32}$$

For large numbers of passage j (see Fig. 11) the shift of the intensity peak position becomes proportional to j and the pulse duration becomes proportional to j^{-1} due to this shift. The peak intensity of optimum pulse shoftening rises proportional to $j (I_{s,s} \propto \Delta t_L^{-1})$.

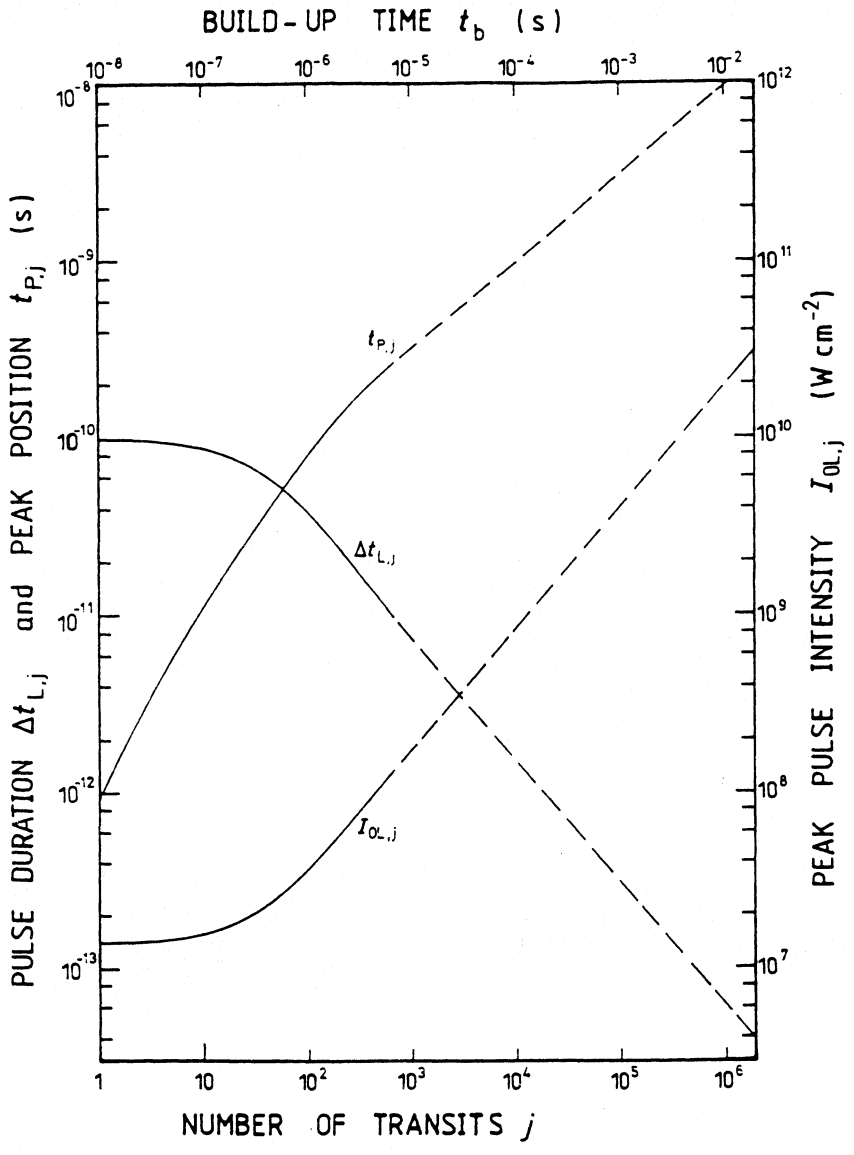

Figure 13 Illustration of asymptotic pulse development in slow saturable absorber. Initial input pulse has Gaussian shape of 100 ps duration. The dye parameters belong to λ_L = 620 nm, T_3 = 1 ps, τ_{FC} = 0.95 ps, and $T_{0,i}$ = 0.9. The jet parameters are v = 7 m s^{-1} and d = 7 μm. The curves are calculated up to 700 transits and then extrapolated. The peak pulse intensity is recovered after each transit according to $I_{0L,j} = 6I_{S,s}(\Delta t_j)$.

In Fig. 12b the pulse shapes after (1) 10, (2) 60 and (3) 100 transits are displayed for an initial pulse duration of 1 ps and a small-signal transmission of T_0 = 0.063. The dye parameters belong to DODCI at 620 nm. The dashed curves belong to $T_3 = \tau_{FC}$ = 1 ns. The decaying shapes agree reasonably well with the shapes of Fig. 12a. The solid curves are calculated for T_3 = 1 ps and τ_{FC} = 0.95 ps. The enhanced pulse shortening and the steepening of the pulse shapes due to the partial fast absorption recovery are clearly seen.

The pulse development in many round trips for an initial Gaussian pulse of 100 ps duration and an initial small-signal transmission of $T_{0,i}$ = 0.9 is illustrated in Fig. 13. The laser wavelength is set to 620 nm with T_3 = 1 ps and τ_{FC} = 0.95 ps. The laser peak intensity

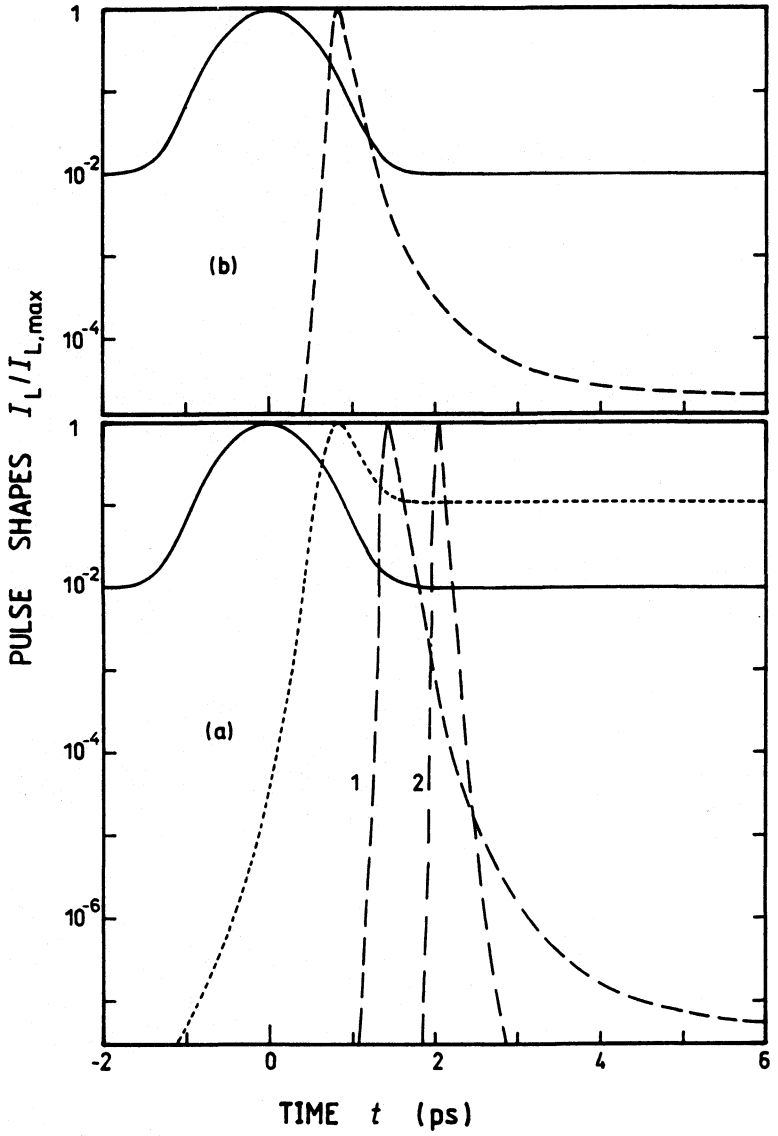

Figure 14 Influence of background level on pulse development. Initial input pulse shape is shown by (——) curves. The dye parameters belong to λ_L = 620 nm and $I_{0L,j} = 6I_{S,s}(\Delta t_j)$. (a) $T_{0,i}$ = 0.063. (– – –) curves: T_3 = 1 ps and τ_{FC} = 0.95 ps. (1) 20 transits and (2) 40 transits. (- - -) curve: $T_3 = \tau_{FC}$ = 1 ns, 6 transits; (b) $T_{0,i}$ = 0.9. (— — —) curve: T_3 = 1 ps, τ_{FC} = 0.95 ps, 200 transits.

is fixed to $I_{0L,j} = 6I_{S,s}$. The curves are calculated up to 700 transits and then extrapolated. For these realistic data of a CPM dye laser the saturable absorber DODCI shortens the pulses from 100 ps to 40 fs in approximately 0.02 s. Here the pulse shaping action of the amplifying dye medium due to gain saturation is not included. Only the pulse energy is kept constant. The laser pulse intensity increases inversely proportional to the shortening. The peak laser intensity needed to start the mode-locking action is $I_{0L} \approx I_{S,f}$ ($\approx 2 \times 10^5$ W cm^{-2} at λ_L = 620 nm). This intensity is reached by focusing of the c.w. laser radiation in the absorber cavity. The pulse shortening is accompanied by a continuous shift of the temporal intensity peak position.

The influence of background intensity on the pulse shortening action in multiple transits is illustrated in Fig. 14a and b. The solid curves represent the initial pulse shapes with $\Delta t_{L,i} = 1$ ps. The dashed curves belong to $T_3 = 1$ ps, $\tau_{FC} = 0.95$ ps, $I_{0L,j} = 6 \times I_{S,s}$, $T_{0,i} = 0.9$ (a) and 0.063 (b). The other dye parameters apply to $\lambda_L = 620$ nm. The continuous reduction of the back-ground level is due to the partial fast absorption recovery of DODCI. The short-dashed curve in Fig. 14a shows the situation for $T_3 = \tau_{FC} = 1$ ns. The other parameters are unchanged. The background suppression is lost (see curves 1 in Fig. 4) and, as the leading part of the circulating pulse is absorbed, the background signal becomes dominant and strong pulse broadening results.

5. Conclusions

The saturable absorption dynamics of DODCI in the wavelength region between 570 and 650 nm in single passages and in repetitive transits has been studied numerically. The photoisomerization dynamics of the N- and P-isomers in the multiple transits leads to an enhanced pulse shortening around 620 nm and to reduced pulse shortening around 590 nm. The slow saturable absorber (slow S_1–S_0-relaxation) shortens continuously the pulses when the absorption losses are compensated by pulse amplification in a gain medium. The fast Franck–Condon relaxation in the S_1-state in the case of short-wavelength excitation and the fast spectral cross-relaxation in the S_0-state in the case of long-wavelength excitation enhance the pulse shortening and are crucial for the background signal suppression.

Here only the pulse shortening action of the saturable absorber was studied. The concerted pulse shaping of the saturable absorber (leading edge absorption) and the gain medium (leading edge amplification) [25–31] in real CPM dye lasers will be studied elsewhere [32].

References

1. W. SCHMIDT and F. P. SCHÄFER, *Phys. Letters* **A26** (1968) 558.
2. D. N. DEMPSTER, T. MORROW, R. RANKIN and G. F. THOMPSON, *J. Chem. Soc. Faraday Trans. II* **68** (1972) 1479.
3. D. J. BRADLEY, in 'Ultrashort Light Pulses', edited by S. L. Shapiro, *Top. in Appl. Phys.* **18** (Springer, Berlin, 1977) p. 18.
4. R. S. ADRIAN, E. G. ARTHURS, D. J. BRADLEY, A. G. RODDIE and J. R. TAYLOR, *Opt. Commun.* **12** (1974) 140.
5. C. V. SHANK, in 'Ultrashort Laser Pulses and Applications', edited by W. Kaiser, *Top. in Appl. Phys.* **60** (Springer, Berlin, 1988) p. 5.
6. G. R. FLEMING, 'Chemical Applications of Ultrafast Spectroscopy' (Oxford University Press, Oxford, 1986).
7. A. PENZKOFER, *Appl. Phys.* **B46** (1988) 43.
8. J. C. DIELS, in 'Dye Laser Principles with Applications', edited by F. J. Duarte and L. W. Hillman (Academic Press, San Diego, 1990) pp. 41.
9. Y. ISHIDA, T. YAJIMA and K. NAGANUMA, *Jpn. J. Appl. Phys.* **19** (1980) L717.
10. J. A. VALDMANIS and R. L. FORK, *IEEE J. Quantum Electron.* **QE-22** (1986) 112.
11. A. FINCH, G. CHEN, W. SLEAT and W. SIBBETT, *J. Mod. Optics* **35** (1988) 345.
12. W. BÄUMLER and A. PENZKOFER, *Chem. Phys. Lett.* **150** (1988) 315.
13. *Idem, Chem. Phys.* **140** (1990) 75.
14. *Idem, ibid.*, **142** (1990) 43.
15. O. E. MARTINEZ, R. L. FORK and J. P. GORDON, *J. Opt. Soc. Am.* **B2** (1987) 1639.
16. V. PETROV, W. RUDOLPH and B. WILHELMI, *Rev. Phys. Appl.* **22** (1987) 1639.
17. W. BLAU, W. DANKESREITER and A. PENZKOFER, *Chem. Phys.* **85** (1984) 473.
18. A. PENZKOFER and P. SPERBER, *Chem. Phys.* **88** (1984) 309.
19. S. DÄHNE, D. LEUPOLD and H. STIEL, *Acta Phys. Polon.* **A71** (1987) 777.
20. A. PENZKOFER and W. BLAU, *Opt. Quantum Electron.* **15** (1983) 325.

21. G. ANGEL, R. GAGEL and A. LAUBEREAU, *Chem. Phys.* **131** (1989) 129.
22. C. RULLIERE, *Chem. Phys. Lett.* **43** (1976) 303.
23. J. JARAUDIAS, *J. Photochem.* **13** (1980) 35.
24. A. SEILMEIER and W. KAISER, in 'Ultrashort Laser Pulses and Applications', edited by W. Kaiser, *Top. in Appl. Phys.*, **60** (Springer-Verlag, Berlin, 1988) p. 279.
25. G. H. C. NEW, *IEEE J. Quantum Electron.* **QE-10** (1974) 115.
26. G. H. C. NEW and D. H. REA, *J. Appl. Phys.* **47** (1976) 3107.
27. B. GARSIDE and T. LIM, *Opt. Commun.* **12** (1974) 8.
28. H. HAUS, *IEEE J. Quantum Electron.* **QE-11** (1975) 736.
29. J. HERRMANN, F. WEIDNER and B. WILHELMI, *Appl. Phys.* **B26** (1981) 197.
30. M. S. STIX and E. P. IPPEN, *IEEE J. Quantum Electron.* **QE-19** (1983) 520.
31. J. D. SIMON, *Rev. Sci. Instrum.* **60** (1959) 3597.
32. A. PENZKOFER and W. BÄUMLER, *Opt. Quantum Electron.*, to be published.